



# Enhanced structure and surface stability of high-nickel cathode materials by $\text{AlPO}_4$ modification

Shuaiwei Liu<sup>1,2</sup> · Shenghong Chang<sup>1,2</sup> · Yunjiao Li<sup>1,2</sup> · Jiachao Yang<sup>1,2</sup> · Zhouliang Tan<sup>1,2</sup> · Xugang Ren<sup>1,2</sup> · Yike Xiong<sup>1,2</sup> · Shan Wang<sup>1,2</sup> · Xiaoming Xi<sup>3</sup> · Zhenjiang He<sup>1,2</sup>

Received: 26 February 2022 / Revised: 6 June 2022 / Accepted: 27 June 2022 / Published online: 13 July 2022  
© The Author(s), under exclusive licence to Springer-Verlag GmbH Germany, part of Springer Nature 2022

## Abstract

High-nickel material is a high energy density cathode. However, its practical application is hindered by the structure and surface instability that cause severe capacity fading during cycling. In this study, a one-step approach of  $\text{AlPO}_4$  modification to create  $\text{Li}_3\text{PO}_4$ - $\text{LiAlO}_2$  coating layer on  $\text{LiNi}_{0.8}\text{Co}_{0.1}\text{Mn}_{0.1}\text{O}_2$  cathode materials is reported. The  $\text{Li}_3\text{PO}_4$ - $\text{LiAlO}_2$  protective coating can not only mitigate the structure degradation near the surface, but also protect from the attacking of HF and  $\text{H}_2\text{O}$  to the bulk surface. The  $\text{AlPO}_4$ -modified materials exhibit excellent electrochemical properties, where its initial discharge capacity is up to  $190.2 \text{ mAh g}^{-1}$  at 1C over 3.0–4.4 V, and the corresponding retention after 100 cycles also increases to 96.42%. Overall, this work offers some meaningful insights on addressing the structure and surface instability, and enhancing the properties of high-nickel materials, which can be of great importance for the further development and commercialization of high-nickel materials.

**Keywords** Lithium-ion batteries · High-nickel ·  $\text{AlPO}_4$  · Coating

## Introduction

Driven by the issues of energy and environment, electric vehicles (EVs) are attracting much attention from the world [1, 2]. Lithium ion batteries (LIBs), with the advantages of long-life and high-energy density, are considered as one of the most promising power batteries [3, 4]. At present, ternary cathode materials ( $\text{LiNi}_x\text{Co}_y\text{M}_z\text{O}_2$ ,  $M = \text{Al, Mn, x} + y + z = 1$ ) have been widely applied in EVs, due to their higher energy density, and lower cost compared with lithium cobalt oxides (LCO), especially the series of NCM622 and NCM523 [5]. Despite the cost having been declined to some extent, the expensive cost of lithium and cobalt and the large demand of high-energy density EVs, still push the cathode to

gradually develop to the ternary materials with much higher nickel content ( $x > 0.6$ ) [6]. However, the wider application of high-nickel ternary materials in EVs, is hindered by its severe capacity fading and potential safety issues during cycles, due to its intrinsic structure and surface instability [7, 8]. The materials in the charge/discharge process suffer sequential phase transformation, structure instability easy to make the phase transformation irreversible, while surface instability meaning that the material surface is easy to react with the electrolyte causing severe phase degradation on surface [9, 10]. Meanwhile, the phase degradation or the reaction between the material surface and electrolyte is also possibly accompanied with gas release ( $\text{O}_2$ ,  $\text{H}_2\text{O}$  and  $\text{CO}_2$ ), making the batteries swollen and even explode [11]. Therefore, it is why structure and surface instability are supposed to take most reasons for the capacity fading and safety issues.

Great efforts have been done for these troubles. Lin et al. developed nickel concentration-gradient materials to enhance the cathode cycling stability [12]. They found that the structure and surface stability could be effectively improved by introducing Ni-valence gradient from the surface to center of the secondary particle of high-nickel-content material, and thus the materials performed

✉ Yunjiao Li  
yunjiao\_li@csu.edu.cn

<sup>1</sup> School of Metallurgy and Environment, Central South University, Changsha 410083, People's Republic of China

<sup>2</sup> Engineering Research Center of the Ministry of Education for Advanced Battery Materials, Central South University, Changsha 410083, People's Republic of China

<sup>3</sup> Changsha Research Institute of Mining and Metallurgy, Changsha 410083, People's Republic of China

better electrochemical properties. Zheng et al. achieved the enhancement of interface stability of  $\text{LiNi}_{0.8}\text{Co}_{0.1}\text{Mn}_{0.1}\text{O}_2$  materials by  $\text{In}_2\text{O}_3$  &  $\text{LiInO}_2$  co-coating. The coating layer can alleviate the sensitivity of high-nickel materials to  $\text{H}_2\text{O}$  and  $\text{CO}_2$  in air and prevent from the attacking of HF during cycling, and thus enables a better electrochemical property [13]. Liu et. al. studied the dual-modified effects of  $\text{Ta}_2\text{O}_5$  on  $\text{LiNi}_{0.8}\text{Co}_{0.15}\text{Al}_{0.05}\text{O}_2$  cathode, and found that the created  $\text{Ta}_2\text{O}_5$  coating layer could effectively protect the materials surface and improve the stability, while the doped  $\text{Ta}^{5+}$  in the bulk could mitigate the cation mixing and stabilize the bulk structure, so the electrochemical properties exhibit a remarkable improvement [14].

Overall, the goal of this study is expected to explore more possibility on improving the surface and structure stability of  $\text{LiNi}_{0.8}\text{Co}_{0.1}\text{Mn}_{0.1}\text{O}_2$  cathode materials. In this study,  $\text{AlPO}_4$  modification is achieved in one step of solid-state method, obtaining  $\text{Li}_3\text{PO}_4$ - $\text{LiAlO}_2$  coated high-nickel materials. With a full and deep investigation, it is found that the modification strategy is available to enhance the structure and surface stability, and enables a better electrochemical property of high-nickel materials. Therefore, it is believed that this modification strategy could have attached enough attention to the further development of LIBs.

## Experimental

### Materials synthesis

The precursor  $\text{Ni}_{0.8}\text{Co}_{0.1}\text{Mn}_{0.1}(\text{OH})_2$  (Ningbo Jinhe New Material Co., LTD),  $\text{LiOH}\cdot\text{H}_2\text{O}$  and  $\text{AlPO}_4$  were evenly mixed in a mixing apparatus, with a molar ratio  $\text{Ni}_{0.8}\text{Co}_{0.1}\text{Mn}_{0.1}(\text{OH})_2/\text{LiOH}\cdot\text{H}_2\text{O}$  of 1:1.07, and a mass

ratio  $\text{AlPO}_4/\text{Ni}_{0.8}\text{Co}_{0.1}\text{Mn}_{0.1}(\text{OH})_2$  of 0, 2500, 3500, and 4500 ppm, respectively. This calcining process and the corresponding chemical reaction are shown in Fig. 1 [15, 16], in order to better understand this process. Then, the mixed powder was calcined at  $550\text{ }^\circ\text{C}$  for 4 h followed by  $800\text{ }^\circ\text{C}$  for 12 h under oxygen atmosphere, to obtain  $\text{Li}_3\text{PO}_4$ - $\text{LiAlO}_2$ -coated high-nickel materials. The obtained materials were marked as Pristine, AP-2500, AP-3500, and AP-4500 according to the dosage of  $\text{AlPO}_4$ .

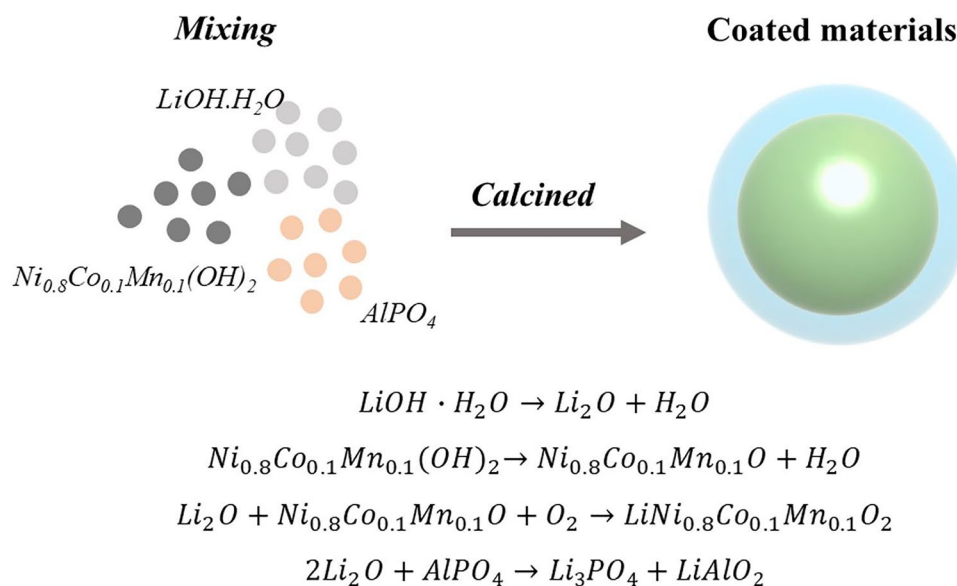
### Material characterization

The composition, structure and morphology of the samples were conducted by the following characterizations: X-ray photoelectron spectrometer (XPS, Thermo ESCALAB 250XI), X-Ray Diffraction (XRD, PANalytical/Empryan 2), scanning electron microscope (SEM, Japan Electronics /JSM-7900F) coupled with Energy Disperse Spectroscopy (EDS, USA/EDAX), transmission electron microscope (TEM, FEI Tecnai G2 F20).

### Electrochemical measurement

The active materials (80 wt.%), the polyvinylidene fluoride (PVDF, 10 wt.%) and the acetylene black (10 wt.%) were evenly mixed in N-methyl-2-pyrrolidone (NMP). Then, the mixed slurry was uniformly coated on an aluminum foil and then dried in vacuum drying oven at  $90\text{ }^\circ\text{C}$  for 6 h. The CR2016 coin half-cells were assembled in a glovebox filled with argon. The electrolyte was the mixture of  $\text{LiPF}_6$  (1 M), ethylene carbonate (EC)/dimethyl carbonate (DMC) and ethyl methyl carbonate (EMC) (volume ratio 1:1:1). The electrochemical test was tested by Land Battery Test System and Princeton Electrochemical

**Fig. 1** Diagram of synthesis mechanism of  $\text{AlPO}_4$ -modified materials



Work Station. The charge–discharge test was conducted at the thermostatic tank of 25 °C, with 0.1 C (1 C = 180 mAh g<sup>-1</sup>) for one cycle, 0.5 C for one cycle and then 1 C for cycles, and the voltage range was from 3.0 to 4.4 V. In the rate tests, the cells were firstly charged to 4.4 V with the rate of 0.1 C, 0.5 C, 1 C distinctively, and then discharged to 3.0 V with the rate of 0.1 C, 0.5 C, 1 C, 2 C, 4 C, 8 C and 0.5 C, respectively. The cyclic voltammetry cycles (CV) were performed under 0.1 mV s<sup>-1</sup> and over 3.0–4.4 V. The electrochemical impedance spectroscopy (EIS) was carried out with frequency from 0.01 to 100 kHz, and the battery state of charge is 4.4 V. The cycled batteries were disassembled in a glovebox, and the electrodes were washed with diethyl carbonate (DEC).

## Results and discussion

The material morphologies are displayed in Fig. 2 (a–d). All the samples have a spherical morphology that is composed of many smaller particles called primary particle, and the diameter of the second particles are about 15–20 μm. There is slight difference of morphology among these samples, so it is believed that the AlPO<sub>4</sub> modification almost does not influence the sample morphologies during the calcining process. Besides, the displayed EDS figures of AP-3500 correspond to Fig. 2 (b), to have an understanding on the distribution of the main elements on the materials surface. As can be seen, all the elements are uniformly distributed on the materials surface. Despite the elements Al and P are a more tenuous distribution, the co-existence of Al and P on the materials surface can still be preliminarily confirmed. Figure 3 (a–b) exhibits TEM images of AP-3500, and here

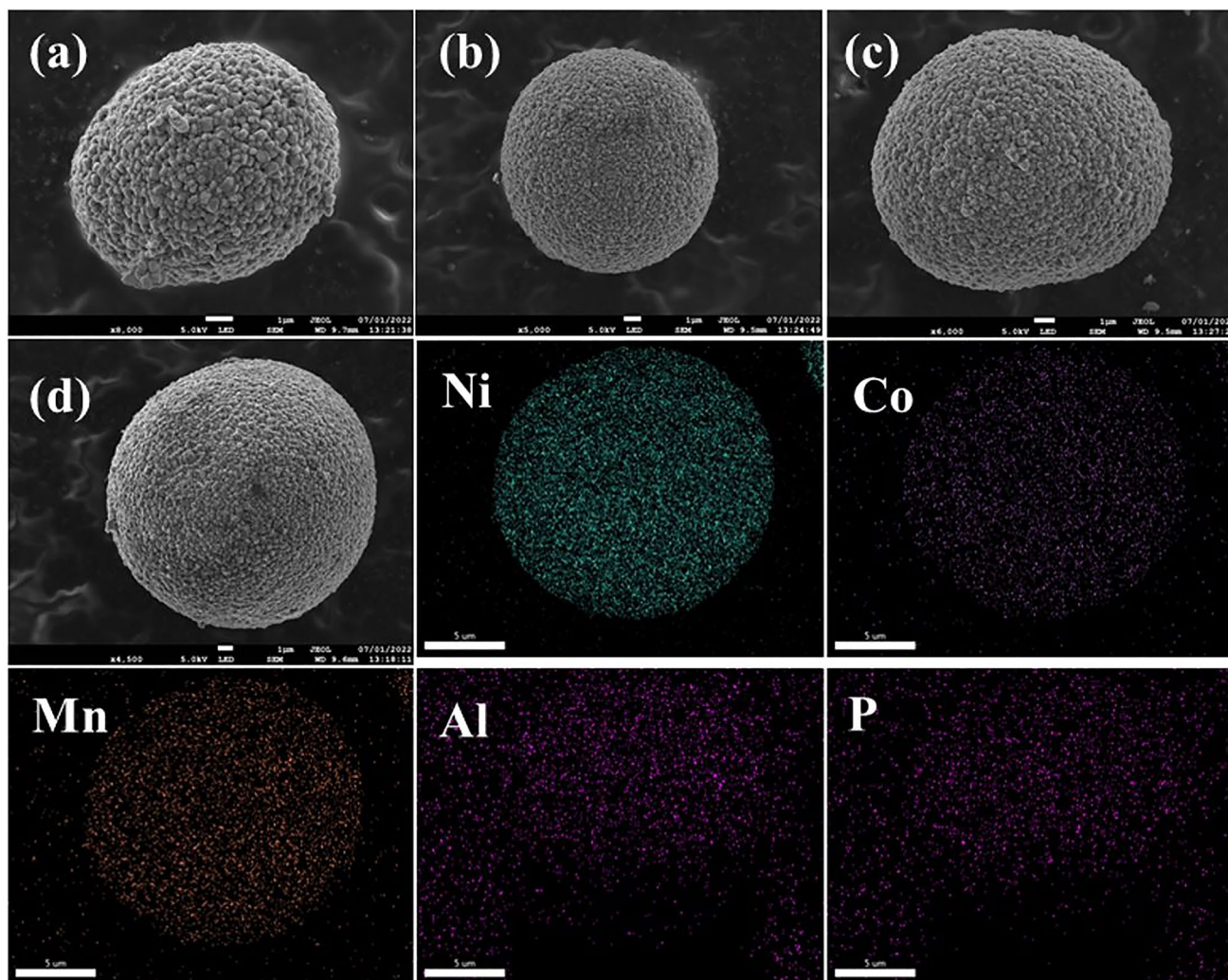
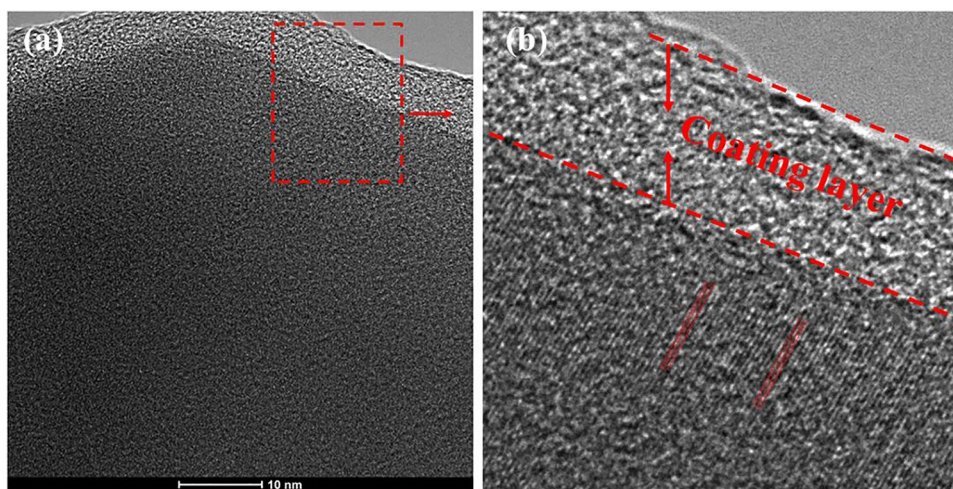


**Fig. 2** SEM images of (a) Pristine, (b) AP-2500, (c) AP-3500, and (d) AP-4500; EDS elemental mapping for AP-3500



**Fig. 3** TEM images of AP-3500 at different multiples



a coating layer with a thickness of 2–3 nm can be obviously seen. Therefore, it can be confirmed that the coating materials can be obtained with Al modification via this method, and the coating performs evenly distributing.

To clear the composition of the coating layer, XPS tests were carried out and the corresponding results are exhibited in Fig. 4 (a–f). At Fig. 4 (a), the peak at 73.2 eV is linked to Al elements. It is reported that the peak related to  $\text{AlPO}_4$  should be located at a higher binding energy site than that of  $\text{LiAlO}_2$  [17]. Generally, the binding energy of the  $\text{AlPO}_4$  peak in Al 2p is about 74.5 eV, while that for  $\text{LiAlO}_2$  is close to 73.4 eV, and thus it is confirmed that the peak in Fig. 4 (a) is assigned to  $\text{LiAlO}_2$  [18]. Besides, the binding energy of the  $\text{AlPO}_4$  peak in P 2p is near 134.4 eV, also higher than that for  $\text{Li}_3\text{PO}_4$  of 133.2 eV. It can be seen that the peak in Fig. 4 (b) is about 133.6 eV, and thereby it is no doubt this peak should be assigned to  $\text{Li}_3\text{PO}_4$  [17–19]. Therefore, we can confirm that the existence state of Al and P elements on the surface is supposed to be  $\text{LiAlO}_2$  and  $\text{Li}_3\text{PO}_4$ , and the coating layer is composed of them.

Additionally, the state of C, O, and Ni is also carefully studied, in order to clear the composition changes on the surface before and after the  $\text{AlPO}_4$  modification. In Fig. 4 (c), the peaks at about 290.2 eV can be assigned to C=O bond, corresponding to  $\text{Li}_2\text{CO}_3$  [20]. By calculating and comparing the peak area of C=O and C–C, the relative proportion of C=O peak area is 23.3% for AP-3500 and 40.4% for Pristine. The result indicates that the amount of  $\text{Li}_2\text{CO}_3$  has an obvious decline after  $\text{AlPO}_4$  modification. As we have all known, the residual lithium salt ( $\text{Li}_2\text{CO}_3$ ,  $\text{LiOH}$ ) is one of the origins deteriorating the electrochemical properties. Its emergence is attributed to the surface instability of the high-nickel materials, which leads to the reduction of the surface  $\text{Ni}^{3+}$  to  $\text{Ni}^{2+}$  separating out the  $\text{Li}_2\text{O}$ , and the  $\text{Li}_2\text{O}$  further reacts with  $\text{H}_2\text{O}$  or  $\text{CO}_2$  in air to generate  $\text{LiOH}$  or  $\text{Li}_2\text{CO}_3$  [21, 22]. Therefore, it can be concluded that the

created coating layer of  $\text{Li}_3\text{PO}_4$ - $\text{LiAlO}_2$  by  $\text{AlPO}_4$  modification has a positive effect on protecting the material surface and inhibiting the structure degradation when it exposes to the ambient air. Additionally, the O 1s spectra also implies the same results. At Fig. 4 (d), AP-3500 exhibits a higher amount of metal oxide bond compared with Pristine, which indicates the lesser residual lithium salts on AP-3500 surface [23]. Furthermore, the valence change of Ni at the material surface is compared by differentiating and imitating the peak of Ni 2p. As shown in Fig. 4 (e) and (f), it can be discovered that the amount of  $\text{Ni}^{3+}$  at the surface for AP-3500 is obviously higher than that of Pristine, which further explains that the created coating layer is beneficial to stabilizing the surface structure.

and (f) Ni 2p of Ap-3500.

Besides, the crystal structure of the samples is determined by XRD, as shown in Fig. 5 (a–b). The diffraction peaks of all samples are well matched with the  $\alpha$ - $\text{NaFeO}_2$  structure and the  $R\bar{3}m$  space group. The clear splitting of (006)/(102) and (008)/(110) indicates that all samples have a well-ordered layer structure [24]. There is no impurity peak in the entire scan range, and there is hardly any shift of (003) peaks among all the samples, which implies that the  $\text{AlPO}_4$  modification just has a slight influence on the main structure of materials. The cell parameters are calculated by Jade software, and the results are listed in Table 1. The cell parameters also do not show obvious changes before and after  $\text{AlPO}_4$  modification, confirming the slight influence of the  $\text{AlPO}_4$  modification on the materials structure. Additionally, all the values of  $c/a$  are bigger than 4.9, explaining their well-ordered layer structure again.

The electrochemical properties of the samples are exhibited in Fig. 6 (a–d), and parts of the corresponding data are summarized in Table 2. Figure 6 (a) displays the initial charge/discharge curves, where all samples have stable charge and discharge platforms. The initial Column

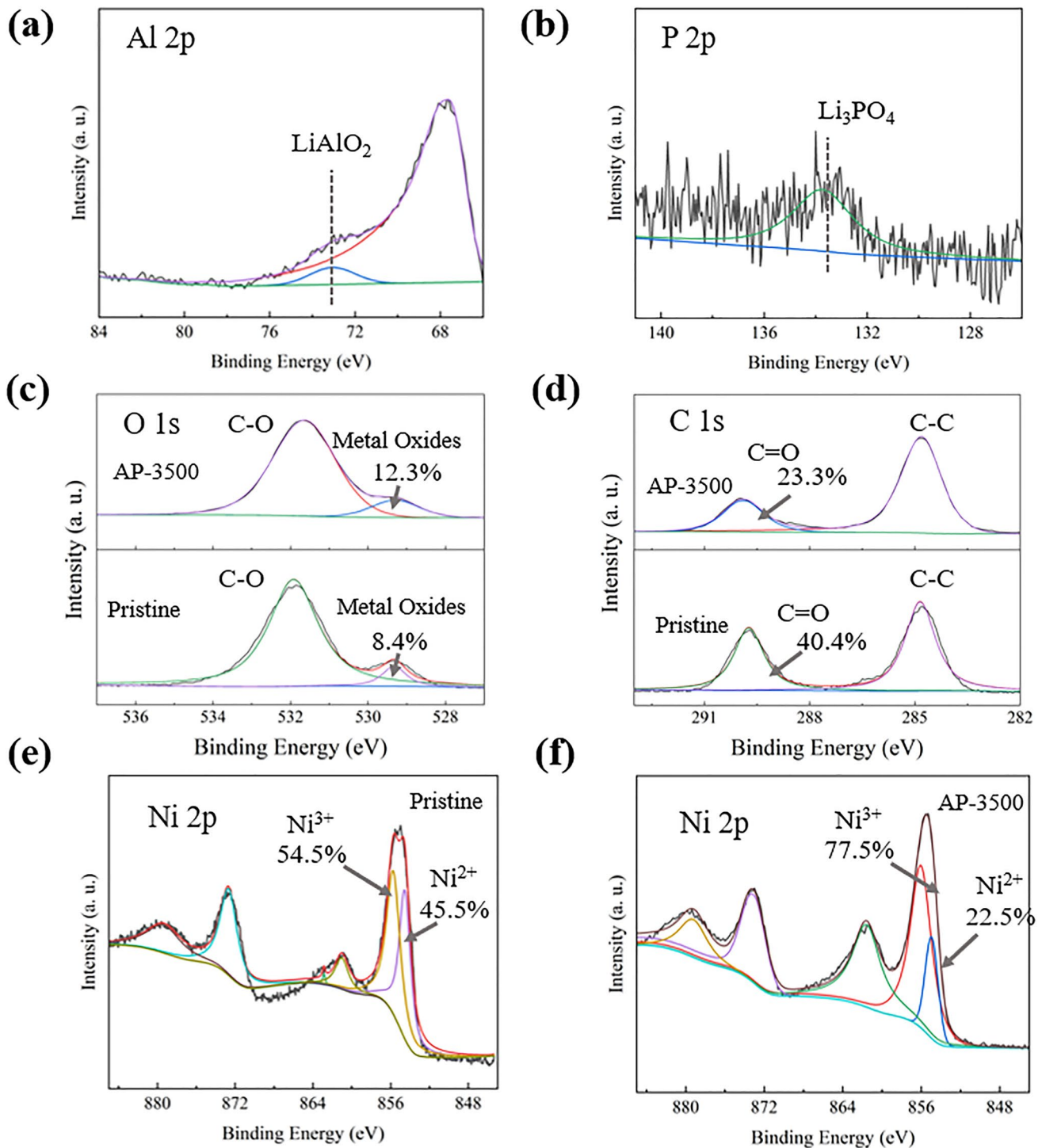


**Fig. 4** XPS spectra of (a) Al 2p, (b) P 2p, (c) C 1 s, (d) O 1 s, (e) Ni 2p of Pristine

Efficiency of Pristine, AP-2500, AP-3500, and AP-4500 is 78.2%, 80.3%, 77.4% and 75.0%, respectively [25]. As we can see, the Column Efficiency declines with an increase of the content of AlPO<sub>4</sub>, which can be because the coating thickness increases as the amount of AlPO<sub>4</sub> becomes higher and higher, and the thicker coating layer is possibly

adverse to the initial de-intercalation process of lithium. The cycling curves under the voltage range from 3.0 to 4.4 V and the rate of 1 C is displayed in Fig. 6 (b). The first discharging specific capacity of Pristine, AP-2500, AP-3500, and AP-4500 is 185.8, 185.2, 190.2, and 179.1 mAh g<sup>-1</sup>, respectively. It can be discovered that the specific capacity

**Fig. 5** XPD patterns of all samples

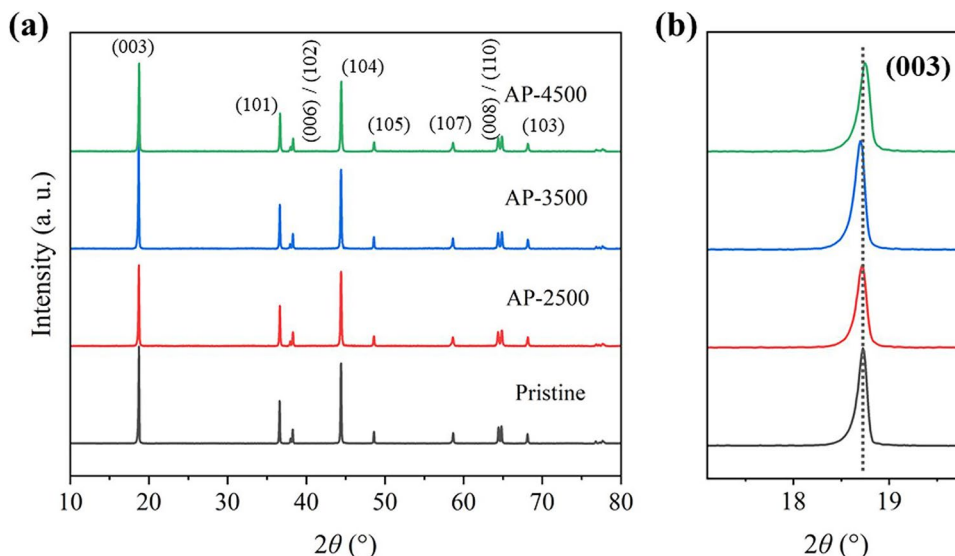


**Table 1** Lattice parameters of all samples

Samples	<i>a</i> (Å)	<i>c</i> (Å)	<i>c/a</i>
Pristine	2.87	14.20	4.94
AP-2500	2.87	14.21	4.95
AP-3500	2.87	14.21	4.95
AP-4500	2.87	14.21	4.95

of AP-3500 has an obvious increase compared with that of Pristine, which can be ascribed to the created coating layer of  $\text{Li}_3\text{PO}_4\text{-LiAlO}_2$  that effectively protects and stabilizes the surface structure. The enhanced surface stability boosts the improvement of the electrochemical properties of the samples. While the decreased capacity of AP-4500 could be attributed to its thicker coating layer, which implies a higher loss of lithium in the previous charge/discharge activation process and thus leads to the decline of capacity. Besides, discharging specific capacity after the 100 cycles of Pristine, AP-2500, AP-3500 and AP-4500 is 156.7, 180.3, 183.4 and 174.8  $\text{mAh g}^{-1}$ , respectively, and the corresponding retention is 84.33%, 97.35%, 96.42%, and 97.60%. It is found that the electrochemical property of AP-3500 has a remarkable improvement for the discharge capacity and the retention, and both the retention of AP-2500 and AP-4500 have an increase as well. Furthermore, the rate curves of the samples are shown in Fig. 6 (c). The discharge capacity of AP-2500, AP-3500, and AP-4500 at the last cycle of 8 C still delivers 165.7, 167.3, and 164.8  $\text{mAh g}^{-1}$ , respectively, while that of Pristine is only 154.7  $\text{mAh g}^{-1}$ , indicating a significant improvement of the rate property after  $\text{AlPO}_4$  modification. Overall, these results are no doubt to explain the superiority of the  $\text{AlPO}_4$  modification on mitigating the capacity fading and enhancing the electrochemical properties, and the material with the additive of 3500 ppm  $\text{AlPO}_4$  performs the

best improvement. The enhancing mechanism of the electrochemical properties can be attributed to the protection effect of the  $\text{Li}_3\text{PO}_4\text{-LiAlO}_2$  coating layer during cycling, which isolates the materials from electrolyte and protects the materials against the attacking of the HF and  $\text{H}_2\text{O}$  [26, 27], and thus improves the material stability during the cycles, as depicted in Fig. 6 (d).

To explore the electrochemical mechanism of the samples in more details, Fig. 7 (a–f) exhibits the CV curves with a voltage range from 3.0 to 4.4 V and a scan speed at  $0.1 \text{ mV s}^{-1}$ , and the differential curves at different cycles. The CV curves all exhibit three pairs of redox peaks that is expected for high-nickel cathode materials [28]. They represent different phase transformation, from hexagonal to monoclinic ( $\text{H1} \rightarrow \text{M}$ ), and then to hexagonal phase ( $\text{M} \rightarrow \text{H2}$ ) and finally to hexagonal phase ( $\text{H2} \rightarrow \text{H3}$ ) [29], as shown in Fig. 7 (a). The  $\Delta E$  is the difference value of the pair of the redox peak, which reflects the reversibility of the batteries to some extent. At the initial three cycles, it can be found that AP-3500 performs a much lower  $\Delta E$  in the first cycles and a smaller shift of voltage among the three cycles, which indicates the better reversibility and stability for the  $\text{AlPO}_4$ -modified materials. Besides, AP-3500 also shows a higher current peak than that of Pristine after 100 cycles. The reversibility and stability of the materials are strongly linked to the phase transformation during cycling. In order to better explore the reversibility of phase transformation, Fig. 7 (e–f) shows the differential curves at different cycles. It is reported that reversibility of the H2-H3 phase transformation is crucial to maintain the stability of material structure. This phase transformation leads to the sudden contraction of the *c*-axis in the materials, and thus its irreversibility will severely damage the materials structure stability and even cause the appearance of microcracks in the materials

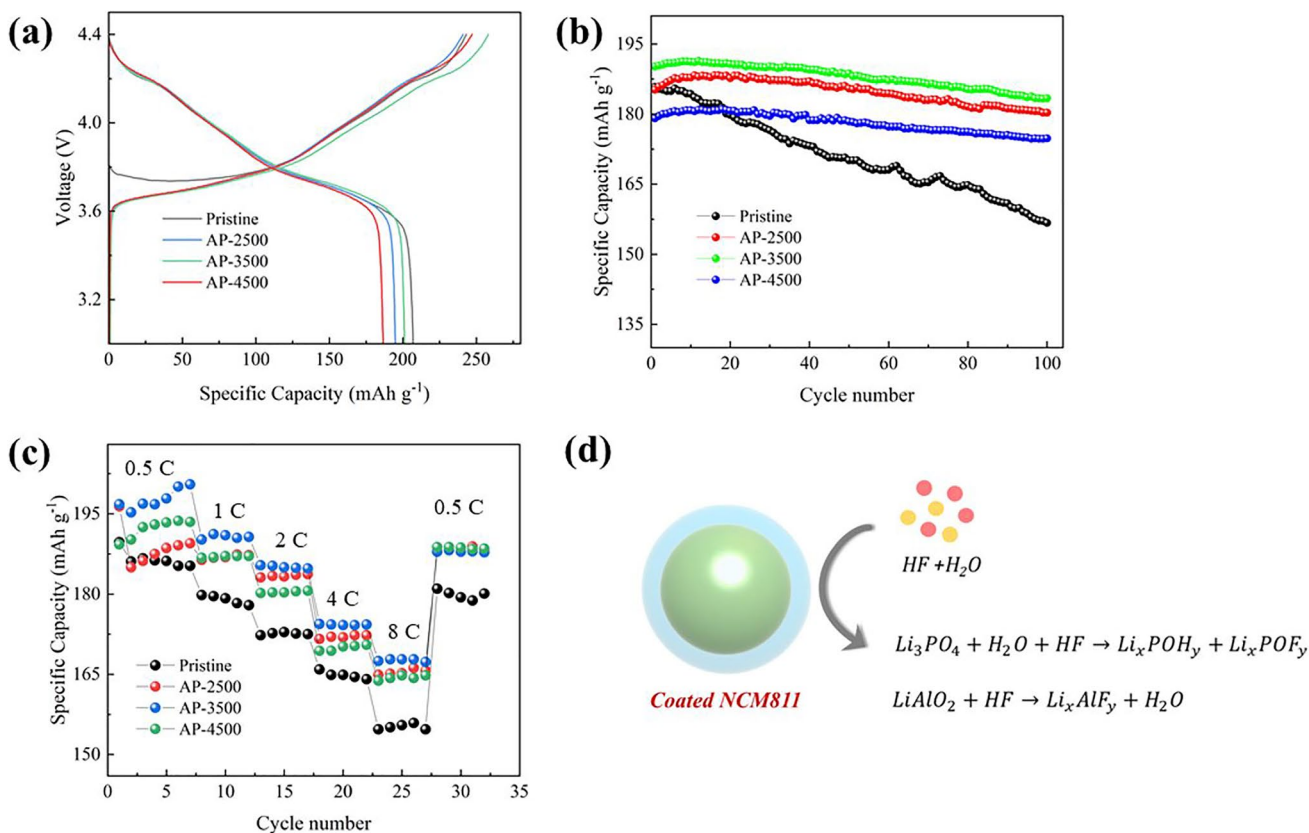


**Fig. 6** (a) Initial charge/discharge curves (0.1 C, 3.0–4.4 V), (b) cycling curves (1 C, 3.0–4.4 V), (c) rate curves of the samples and (d) protection mechanism of the coating layer

**Table 2** Electrochemical data of the samples

Samples	Column efficiency (1 st, 0.1 C) (%)	1 st (1 C, mAh g <sup>-1</sup> )	100 th (1 C, mAh g <sup>-1</sup> )	Retention (%)
Pristine	78.2	185.8	156.7	84.33
AP-2500	80.3	185.2	180.3	97.35
AP-3500	77.4	190.2	183.4	96.42
AP-4500	75.0	179.1	174.8	97.60

[30, 31]. It is obvious that AP-3500 enjoys a much smaller decrease of peak intensity as well as the shift of the peaks compared with that of Pristine, as the cycles are continuing. Besides, after the 100 cycles, the peak of H2-H3 is still clear for AP-3500 while that of Pristine is hardly to find. It can be confirmed again that AlPO<sub>4</sub> modification enables a better reversibility and stability for the materials structure on the basis of these results.

EIS tests were carried out to further illustrate the electrochemical process, as shown in Fig. 8 (a–b). The tested plots consist of two semicircles and a slope line, where the semicircles at high frequency are related to the interface

resistance ( $R_f$ ), while the semicircles at low frequency are linked to the charge-transfer resistance ( $R_{ct}$ ), and the linear part represents the solid-phase activity of Li<sup>+</sup> [32, 33]. The listed impedance results in Table 3 are based on the equivalent circuit diagram that is shown in Fig. 8 (a), and are calculated by using Zview 2.0 software. As we can see, the  $R_f$  and  $R_{ct}$  values of AP-3500 both are lower than that of Pristine, which could be ascribed to the inhibited structure degradation near the surface and the decreased by-product on the surface after the AlPO<sub>4</sub> modification. In addition, it is discovered that the  $R_f$  in the first cycle of the samples is higher than that of the 50th cycles, especially for AP-3500, which can be attributed to the formation process of cathode electrolyte interphase (CEI) that makes the diffusion of lithium more difficult, and it could just appear at the first few cycles, and thus cause the high value of  $R_f$  [25, 34]. Besides, the created Li<sub>3</sub>PO<sub>4</sub>-LiAlO<sub>2</sub> coating layer probably means that the stable process of the CEI will be more complex than Pristine, so the value  $R_f$  is higher than that of Pristine in the first cycle.

In order to get a profound understanding of the materials structure and morphology after the cycles, the characterization of XRD and SEM is implemented, and the



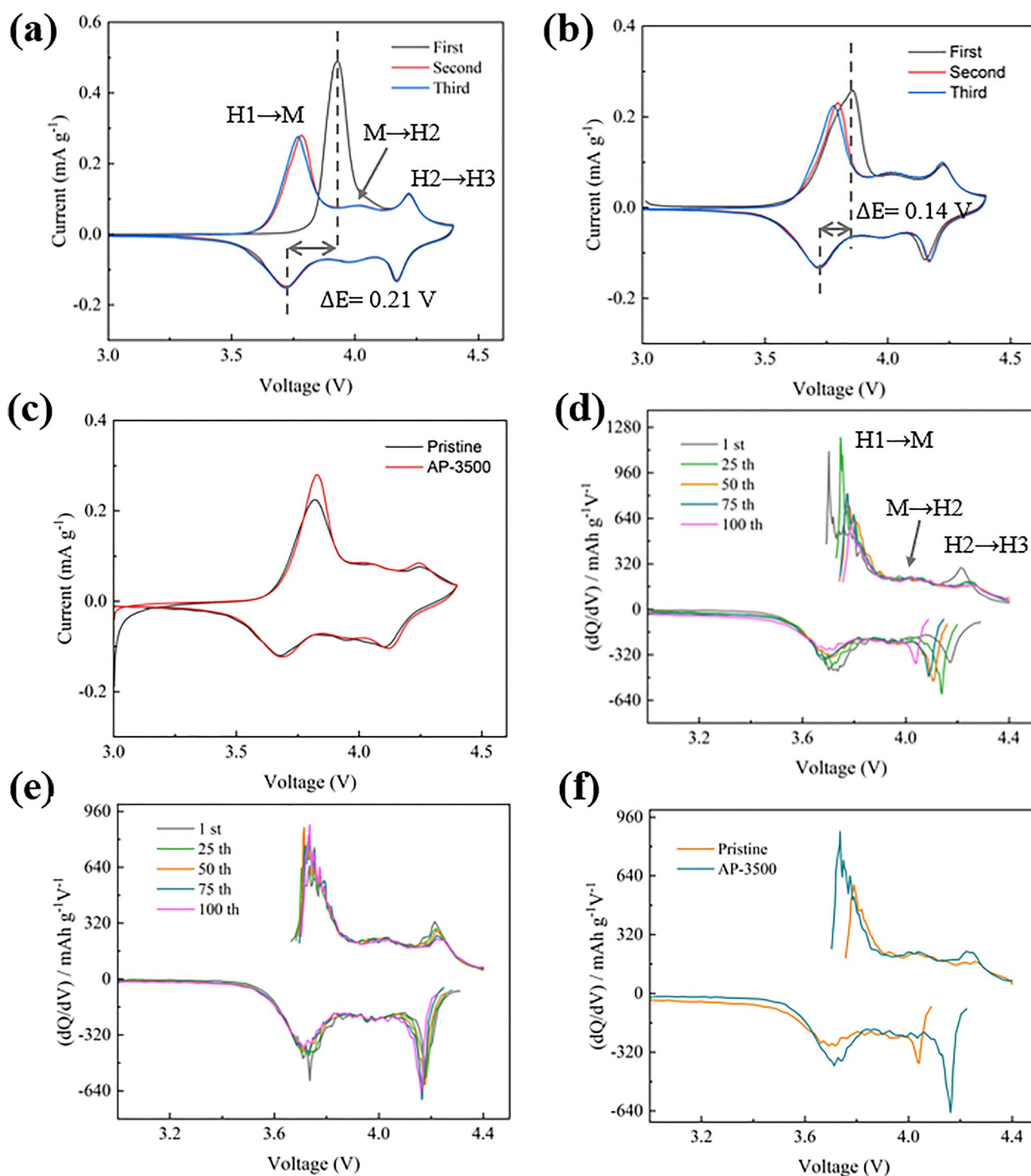


**Fig. 7** CV curves of the initial three cycles of (a) Pristine, (b) AP-3500, (c) CV curves after 100 cycles; Differential curves at different cycles of (d) Pristine, (e) AP-3500 and (f) the comparison of differential curve between Pristine and AP-3500 at 100 cycles

corresponding results are displayed in Fig. 9 (a–d). As can be seen in Fig. 9 (a–b), the cycled materials still maintain the layer structure to certain extent, and there is no other impurity peak observed. Additionally, it is found that the

shift of angles after 100 cycles in AP-3500 is smaller than that of Pristine, explaining that the structure reversibility of AP-3500 is superior to that of the Pristine, which confirms again that the  $\text{AlPO}_4$  modification is beneficial to enhance



**Fig. 8** EIS plots at different cycles of (a) AP-3500, (b) Pristine

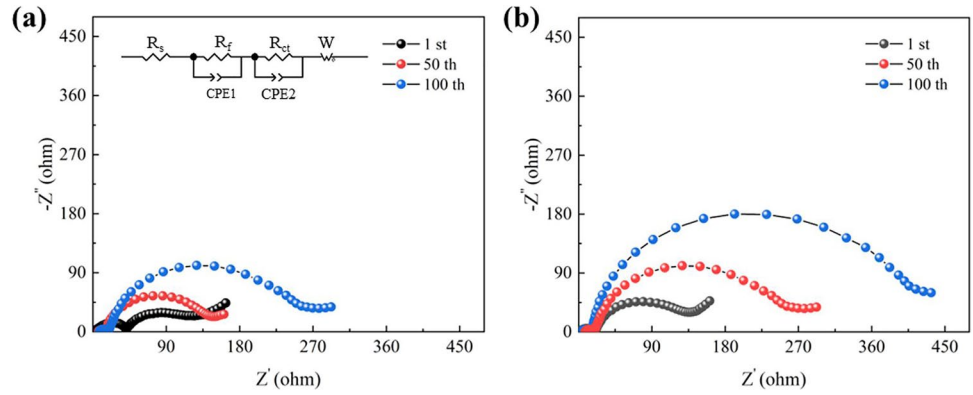
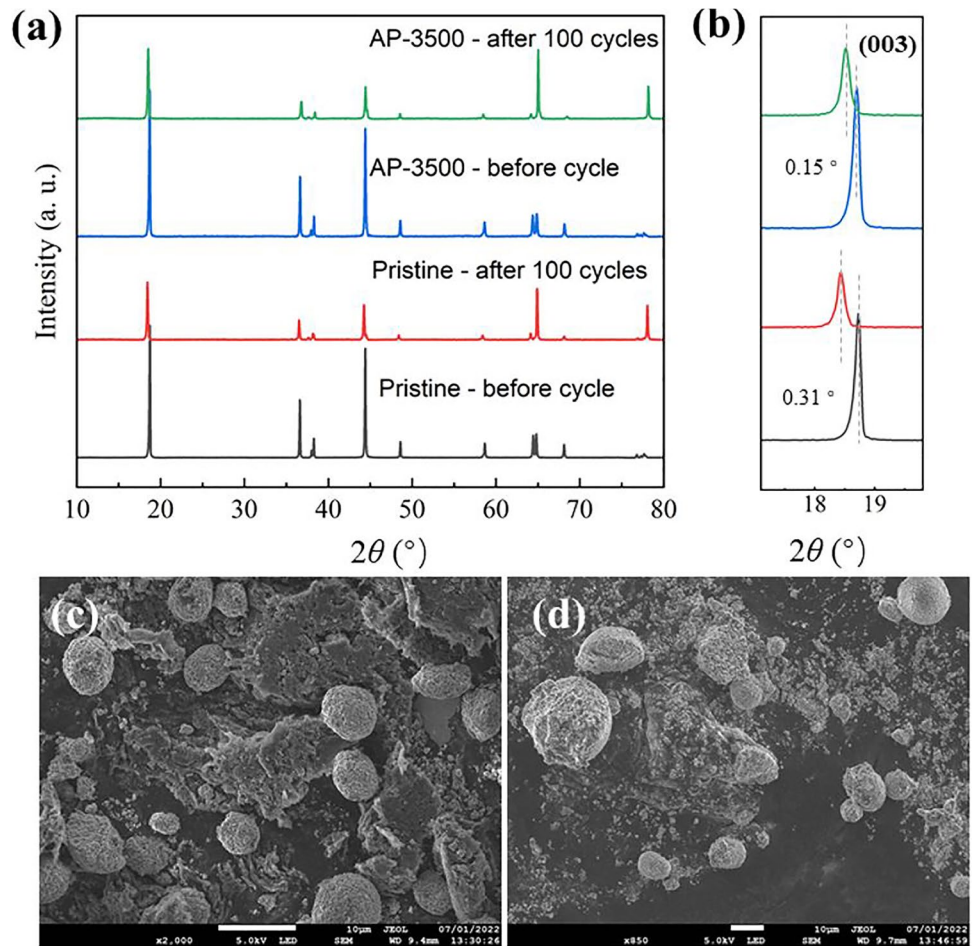


**Table 3** Fitting impedance results based on Fig. 8

Samples	$R_f$ ( $\Omega$ )			$R_{ct}$ ( $\Omega$ )		
	1st	50th	100th	1st	50th	100th
Pristine	38.61	8.05	18.16	14.10	219.30	336.50
AP-3500	63.4	12.09	18.70	63.16	107.90	226.50

**Fig. 9** XRD patterns of Pristine and AP-3500 before and after 100 cycles (a, b); SEM images of (c) AP-3500 and (d) Pristine after 100 cycles



the structure stability of materials [35, 36]. Additionally, it is also observed in Fig. 9 (c–d) that the particle breakage in AP-3500 is effectively mitigated, thanks to the protection effect of the  $\text{Li}_3\text{PO}_4\text{-LiAlO}_2$  coating layer that effectively inhibits the side reaction between the materials and electrolyte. In summary, the  $\text{AlPO}_4$  modification can effectively improve the structure and surface stability, and thus enables the superior cyclability.

## Conclusion

Overall, the electrochemical properties of the high-nickel materials are effectively improved by the  $\text{AlPO}_4$  modification. The initial discharge capacity at 1 C over 3.0–4.4 V of the modified materials AP-3500 can reach 190.2 mAh  $\text{g}^{-1}$ , and the corresponding retention after 100 cycles also increase to 96.42%, both of which are higher than that of the pristine materials (185.8 mAh  $\text{g}^{-1}$ , 84.33%). Besides, the  $\text{AlPO}_4$  modification also enables a better rate property. The discharge capacity at 8 C of AP-3500 is up to 167.3 mAh  $\text{g}^{-1}$ , while that of the pristine materials is only 154.5 mAh  $\text{g}^{-1}$ . Then, we carried out a careful investigation regarding the enhancing mechanism on electrochemical properties of the  $\text{AlPO}_4$  modification. It is found that the improvement of the electrochemical properties benefits from the  $\text{Li}_3\text{PO}_4\text{-LiAlO}_2$  coating layer, which can inhibit the surface structure degradation and protect the materials against the attacking of HF and  $\text{H}_2\text{O}$ , and thus enables a more stable structure and interface for the materials.

**Funding** Thanks for the financial support from Hunan Graduate Scientific Research Innovation Project (No. CX20210204), and Graduate Independent Exploration and Innovation Project of Central South University (No. 2021zzts0600), as well as the Government of Chongzuo, Guangxi Zhuang Autonomous Region (No. FA2020011 and No. 20210713).

## References

- Li M, Lu J, Chen Z, Amine K, (2018) 30 Years of lithium-ion batteries. *Adv Mater*, e1800561 <https://doi.org/10.1002/adma.20180561>
- Whittingham MS (2020) Lithium batteries: 50 years of advances to address the next 20 years of climate issues. *Nano Lett* 20(12):8435–8437. <https://doi.org/10.1021/acs.nanolett.0c04347>
- Cheng XB, Liu H, Yuan H, Peng HJ, Tang C, Huang JQ, Zhang Q (2021) A perspective on sustainable energy materials for lithium batteries. *SusMat* 1(1):38–50. <https://doi.org/10.1002/sus.2.4>
- Eftekhari A (2019) Lithium batteries for electric vehicles: from economy to research strategy. *ACS Sustainable Chemistry & Engineering* 7(6):5602–5613. <https://doi.org/10.1021/acssuschemeng.8b01494>
- Schmich R, Wagner R, Hörpel G, Placke T, Winter M (2018) Performance and cost of materials for lithium-based rechargeable automotive batteries. *Nat Energy* 3(4):267–278. <https://doi.org/10.1038/s41560-018-0107-2>
- Zhou H, Xin F, Pei B, Whittingham MS (2019) What limits the capacity of layered oxide cathodes in lithium batteries? *ACS Energy Lett* 4(8):1902–1906. <https://doi.org/10.1021/acscenergylett.9b01236>
- Ko D, S Park, JH Yu, BY Ahn D, Kim K, Han H, N Jeon, W S Jung C, Manthiram, A (2020) Degradation of high-nickel-layered oxide cathodes from surface to bulk: a comprehensive structural, chemical, and electrical analysis. *Adv Energy Mater* 10(36). <https://doi.org/10.1002/aenm.202001035>
- Li W, Erickson EM, Manthiram A (2020) High-nickel layered oxide cathodes for lithium-based automotive batteries. *Nat Energy* 5(1):26–34. <https://doi.org/10.1038/s41560-019-0513-0>
- Ren X, Li Y, Xi X, Liu S, Xiong Y, Zhang D, Wang S, Zheng J (2021) Modification of  $\text{LiNi}_0.8\text{Co}_0.1\text{Mn}_0.1\text{O}_2$  cathode materials from the perspective of chemical stabilization and kinetic hindrance. *J Power Sources* 499. <https://doi.org/10.1016/j.jpowsour.2021.229756>
- Li T, Yuan X-Z, Zhang L, Song D, Shi K, Bock C (2019) Degradation mechanisms and mitigation strategies of nickel-rich NMC-based lithium-ion batteries. *Electrochem Energy Rev* 3(1):43–80. <https://doi.org/10.1007/s41918-019-00053-3>
- Li J, Zhou Z, Luo Z, He Z, Zheng J, Li Y, Mao J, Dai K (2021) Microcrack generation and modification of Ni-rich cathodes for Li-ion batteries: a review. *Sustain Mater Technol* 29. <https://doi.org/10.1016/j.susmat.2021.e00305>
- Lin R, Bak SM, Shin Y, Zhang R, Wang C, Kisslinger K, Ge M, Huang X, Shadik Z, Pattammattal A, Yan H, Chu Y, Wu J, Yang W, Whittingham MS, Xin HL, Yang XQ (2021) Hierarchical nickel valence gradient stabilizes high-nickel content layered cathode materials. *Nat Commun* 12(1):2350. <https://doi.org/10.1038/s41467-021-22635-w>
- Liu Y, Tang L-b, Wei H-x, Zhang X-h, He Z-j, Li Y-j, Zheng J-c (2019) Enhancement on structural stability of Ni-rich cathode materials by in-situ fabricating dual-modified layer for lithium-ion batteries. *Nano Energy* 65. <https://doi.org/10.1016/j.nanoen.2019.104043>
- Zhang X, Zhang P, Zeng T, Yu Z, Qu X, Peng X, Zhou Y, Duan X, Dou A, Su M, Liu Y (2021) Improving the structure stability of  $\text{LiNi}_0$  by  $8\text{Co}_0.15\text{Al}_0.05\text{O}_2$  Double modification of tantalum surface coating and doping. *ACS Appl Energy Mater* 4(8):8641–8652. <https://doi.org/10.1021/acsaem.1c0181>
- Tang W, Peng Z, Shi Y, Xu S, Shuai H, Zhou S, Kong Y, Yan K, Lu T, Wang G (2019) Enhanced cyclability and safety performance of  $\text{LiNi}_0.6\text{Co}_0.2\text{Mn}_0.2\text{O}_2$  at elevated temperature by  $\text{AlPO}_4$  modification. *J Alloys Compd* 810. <https://doi.org/10.1016/j.jallcom.2019.151834>
- Wang S, Hua W, Missyul A, Darma MSD, Tayal A, Indris S, Ehrenberg H, Liu L, Knapp M (2021) Kinetic control of long-range cationic ordering in the synthesis of layered Ni-rich oxides. *Adv Funct Mater* 31:19. <https://doi.org/10.1002/adfm.202009949>
- Appapillai AT, Mansour AN, Cho J, Shao-Horn Y (2007) Microstructure of  $\text{LiCoO}_2$  with and without “ $\text{AlPO}_4$ ” nanoparticle coating: combined STEM and XPS studies. *Chem Mater* 19(23):5748–5757. <https://doi.org/10.1021/cm0715390>
- Feng Z, Rajagopalan R, Sun D, Tang Y, Wang H (2020) In-situ formation of hybrid  $\text{Li}_3\text{PO}_4\text{-AlPO}_4\text{-Al}(\text{PO}_3)_3$  coating layer on  $\text{LiNi}_0.8\text{Co}_0.1\text{Mn}_0.1\text{O}_2$  cathode with enhanced electrochemical properties for lithium-ion battery. *Chem Eng J* 382. <https://doi.org/10.1016/j.cej.2019.122959>
- Zhou K, Xie Q, Li B, Manthiram A (2021) An in-depth understanding of the effect of aluminum doping in high-nickel cathodes for lithium-ion batteries. *Energy Storage Materials* 34:229–240. <https://doi.org/10.1016/j.ensm.2020.09.015>

20. You Y, Celio H, Li J, Dolocan A, Manthiram A (2018) Modified high-nickel cathodes with stable surface chemistry against ambient air for lithium-ion batteries. *Angew Chem Int Ed Engl* 57(22):6480–6485. <https://doi.org/10.1002/anie.201801533>
21. Jung R, Morasch R, Karayaylali P, Phillips K, Maglia F, Stinner C, Shao-Horn Y, Gasteiger HA (2018) Effect of ambient storage on the degradation of Ni-Rich Positive electrode materials (NMC811) for Li-Ion batteries. *J Electrochem Soc* 165(2):A132–A141. <https://doi.org/10.1149/2.0401802jes>
22. Guan P, Zhou L, Yu Z, Sun Y, Liu Y, Wu F, Jiang Y, Chu D (2020) Recent progress of surface coating on cathode materials for high-performance lithium-ion batteries. *J Energy Chem* 43:220–235. <https://doi.org/10.1016/j.jechem.2019.08.022>
23. Friedrich F, Strehle B, Freiberg ATS, Kleiner K, Day SJ, Erk C, Piana M, Gasteiger HA (2019) Editors' choice—capacity fading mechanisms of NCM-811 cathodes in lithium-ion batteries studied by X-ray diffraction and other diagnostics. *J Electrochem Soc* 166(15):A3760–A3774. <https://doi.org/10.1149/2.0821915jes>
24. Gao S, Zhan X, Cheng Y-T (2019) Structural, electrochemical and Li-ion transport properties of Zr-modified LiNi<sub>0.8</sub>Co<sub>0.1</sub>Mn<sub>0.1</sub>O<sub>2</sub> positive electrode materials for Li-ion batteries. *J Power Sources* 410–411:45–52. <https://doi.org/10.1016/j.jpowsour.2018.10.094>
25. Vortmann-Westhoven B, Winter M, Nowak S (2017) Where is the lithium? Quantitative determination of the lithium distribution in lithium ion battery cells: investigations on the influence of the temperature, the C-rate and the cell type. *J Power Sources* 346:63–70. <https://doi.org/10.1016/j.jpowsour.2017.02.028>
26. Zhu J, Li Y, Xue L, Chen Y, Lei T, Deng S, Cao G (2019) Enhanced electrochemical performance of Li<sub>3</sub>PO<sub>4</sub> modified Li[Ni<sub>0.8</sub>Co<sub>0.1</sub>Mn<sub>0.1</sub>]O<sub>2</sub> cathode material via lithium-reactive coating. *J Alloys Compd* 773:112–120. <https://doi.org/10.1016/j.jallcom.2018.09.237>
27. Kim J, Lee J, Ma H, Jeong HY, Cha H, Lee H, Yoo Y, Park M, Cho J (2018) Controllable solid electrolyte interphase in nickel-rich cathodes by an electrochemical rearrangement for stable lithium-ion batteries. *Adv Mater* 30:5. <https://doi.org/10.1002/adma.201704309>
28. Tang L-B, Liu Y, Wei H-X, Yan C, He Z-J, Li Y-J, Zheng J (2021) Boosting cell performance of LiNi<sub>0.8</sub>Co<sub>0.1</sub>Mn<sub>0.1</sub>O<sub>2</sub> cathode material via structure design. *J Energy Chem* 55:114–123. <https://doi.org/10.1016/j.jechem.2020.06.055>
29. Gan Q, Qin N, Zhu Y, Huang Z, Zhang F, Gu S, Xie J, Zhang K, Lu L, Lu Z (2019) Polyvinylpyrrolidone-induced uniform surface-conductive polymer coating endows Ni-Rich LiNi<sub>0.8</sub>Co<sub>0.1</sub>Mn<sub>0.1</sub>O<sub>2</sub> with enhanced cyclability for lithium-ion batteries. *ACS Appl Mater Interfaces* 11(13):12594–12604. <https://doi.org/10.1021/acsami.9b04050>
30. Jamil S, Wang G, Yang L, Xie X, Cao S, Liu H, Chang B, Wang X (2020) Suppressing H<sub>2</sub>–H<sub>3</sub> phase transition in high Ni–low Co layered oxide cathode material by dual modification. *J Mater Chem A* 8(40):21306–21316. <https://doi.org/10.1039/d0ta07965k>
31. Park K-J, Hwang J-Y, Ryu H-H, Maglia F, Kim S-J, Lamp P, Yoon CS, Sun Y-K (2019) Degradation mechanism of Ni-enriched NCA cathode for lithium batteries: are microcracks really critical? *ACS Energy Lett* 4(6):1394–1400. <https://doi.org/10.1021/acsenergylett.9b00733>
32. Fan Q, Yang S, Liu J, Liu H, Lin K, Liu R, Hong C, Liu L, Chen Y, An K, Liu P, Shi Z, Yang Y (2019) Mixed-conducting interlayer boosting the electrochemical performance of Ni-rich layered oxide cathode materials for lithium ion batteries. *J Power Sources* 421:91–99. <https://doi.org/10.1016/j.jpowsour.2019.03.014>
33. Zha G, Chuying O, Yin S, Yao K, Agarwal S, Hu N, Hou H (2021) High cycling stability of the LiNi<sub>0.8</sub>Co<sub>0.1</sub>Mn<sub>0.1</sub>O<sub>2</sub> cathode via surface modification with Polyimide/multi-walled carbon nanotubes composite coating. *Small* 17(47). <https://doi.org/10.1002/sml.202102981>
34. Zhang Q, Ma J, Mei L, Liu J, Li Z, Li J, Zeng Z (2022) In situ TEM visualization of LiF nanosheet formation on the cathode-electrolyte interphase (CEI) in liquid-electrolyte lithium-ion batteries. *Matter*. <https://doi.org/10.1016/j.matt.2022.01.015>
35. Li J, Downie LE, Ma L, Qiu W, Dahn JR (2015) Study of the failure mechanisms of LiNi<sub>0.8</sub>Mn<sub>0.1</sub>Co<sub>0.1</sub>O<sub>2</sub> Cathode material for lithium ion batteries. *J Electrochem Soc* 162(7):A1401–A1408. <https://doi.org/10.1149/2.1011507jes>
36. Dixit M, Markovsky B, Schipper F, Aurbach D, Major DT (2017) Origin of structural degradation during cycling and low thermal stability of Ni-rich layered transition metal-based electrode materials. *J Phys Chem C* 121(41):22628–22636. <https://doi.org/10.1021/acs.jpcc.7b06122>

**Publisher's Note** Springer Nature remains neutral with regard to jurisdictional claims in published maps and institutional affiliations.